

Finite-Disorder Critical Point in the Yielding Transition of Elastoplastic Models

Saverio Rossi^{1,*}, Giulio Biroli², Misaki Ozawa², Gilles Tarjus¹, and Francesco Zamponi²

¹*LPTMC, CNRS-UMR 7600, Sorbonne Université, 4 Place Jussieu, F-75005 Paris, France*

²*Laboratoire de Physique de l'Ecole Normale Supérieure, ENS, Université PSL, CNRS, Sorbonne Université, Université Paris Cité, F-75005 Paris, France*

 (Received 23 May 2022; accepted 20 October 2022; published 23 November 2022)

Upon loading, amorphous solids can exhibit brittle yielding, with the abrupt formation of macroscopic shear bands leading to fracture, or ductile yielding, with a multitude of plastic events leading to homogeneous flow. It has been recently proposed, and subsequently questioned, that the two regimes are separated by a sharp critical point, as a function of some control parameter characterizing the intrinsic disorder strength and the degree of stability of the solid. In order to resolve this issue, we have performed extensive numerical simulations of athermally driven elastoplastic models with long-range and anisotropic realistic interaction kernels in two and three dimensions. Our results provide clear evidence for a finite-disorder critical point separating brittle and ductile yielding, and we provide an estimate of the critical exponents in 2D and 3D.

DOI: [10.1103/PhysRevLett.129.228002](https://doi.org/10.1103/PhysRevLett.129.228002)

Yielding of amorphous materials is a practically and scientifically important problem [1–5]. When a material is mechanically slowly driven from an initial quiescent glassy state, two different types of yielding behavior are observed. One is brittle yielding, where the sample catastrophically breaks into pieces and displays one or several macroscopic shear bands (usually experimentally encountered in atomic and molecular glasses). The other one is ductile yielding, for which the sample deforms rather homogeneously via a series of local and mesoscopic plastic events that prevent catastrophic failure (usually experimentally encountered in soft materials like colloids and pastes). It has been established that a given material may show brittle or ductile yielding depending on the preparation history of the sample [3,6–8]. In particular, a well-annealed, hence stable, glass sample shows brittle yielding, whereas a poorly annealed, less stable, glass sample exhibits ductile yielding. Note that in the materials science and engineering communities the yield point is traditionally defined as the end of the purely elastic branch and the onset of plastic behavior. However, because several molecular simulations and elastoplastic model (EPM) studies (see, e.g., [9–11]) demonstrated that a purely elastic branch does not exist in sheared amorphous solids as plasticity appears for any infinitesimal deformation in the thermodynamic limit, the statistical physics community usually adopts a different definition of yielding.

Recent theoretical studies suggest that brittle yielding corresponds to a nonequilibrium first-order transition (or spinodal [12–17]), associated with a macroscopic discontinuous stress drop at a given strain value, whereas ductile yielding corresponds to a continuous stress-strain curve, corresponding to a progressive plastic softening of the material. In athermal quasistatic (AQS) conditions [18], it

was observed that these two distinct behaviors are separated by a critical value of the stability (or the disorder) [19–21]. It was then proposed that the brittle-to-ductile transition is a novel nonequilibrium phase transition, similar to that of an athermally driven random-field Ising model [22,23]. Further understanding the transformation from brittle to ductile yielding appears as a major challenge in many fields, from materials science to statistical physics [24–35].

The above scenario has been challenged in Refs. [36–38]. In particular, Ref. [36] argues that in AQS condition and provided the samples are large enough, yielding always takes place in a brittle manner. This should happen irrespectively of the stability or disorder of the samples, except for the putative infinitely disordered sample, thereby implying that the brittle-to-ductile transition does not exist in the thermodynamic limit. Large-scale molecular simulations [38] seem to give some support to the statements of Refs. [36,37]. Yet, it remains hard to conclude due to the limited system sizes accessible in molecular simulations and the very small number of samples involved.

In this Letter, in order to overcome this difficulty and obtain conclusive results, we perform a thorough numerical analysis of the brittle-to-ductile transition in EPMs [1,39]. These mesoscopic models have already been successfully applied to describe several aspects of the rheology of amorphous materials, in particular the yielding transition [37,40]. Their coarse-grained lattice nature enables us to access very large system sizes and a large number of samples, allowing for a careful finite-size scaling analysis of the critical point. Our main result is direct numerical evidence for the existence of a finite-disorder critical point separating brittle and ductile behavior.

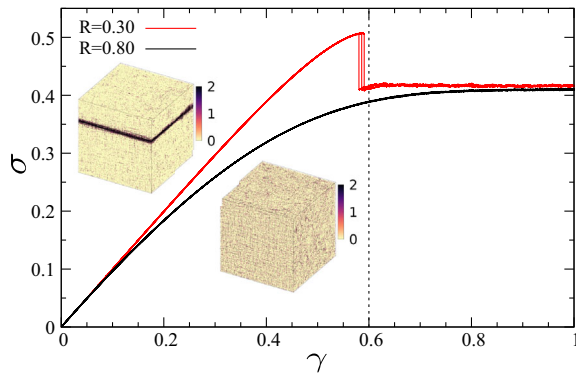


FIG. 1. Stress versus strain curves in the 3D elastoplastic model illustrating the brittle ($R = 0.3$) and the ductile ($R = 0.8$) cases. The linear box length is $L = 200$. Three independent samples are presented. Insets: Real-space configurations at $\gamma = 0.6$ in the two cases. The color bar corresponds to the number of local plastic events.

The type of EPM we focus on provides a simple scalar description of the AQS dynamics [41–43] and corresponds to a cellular automaton on two-dimensional (2D) and three-dimensional (3D) cubic lattices. In particular, we consider incompressible, homogenous, and isotropic materials under a simple shear deformation protocol and we focus on a single shear-stress component that we denote σ [39]. (This is an approximate treatment which ignores the other stress components.) The model describes the evolution of coarse-grained local stresses σ_i in the presence of an external strain γ . Whenever one such stress goes above a stability threshold, the site yields, and the resulting stress drop is propagated through the sample via a long-range Eshelby-like propagator [44]. The initial stability of the solid, which in real systems depends on the annealing protocol, is quantified by a parameter R associated with the width of the initial stress distribution (and therefore characterizing the strength of the disorder). We vary the system size over a wide range of linear box lengths, $L = 256$ – 4096 for 2D and $L = 48$ – 164 (with a few samples at $L = 200$) for 3D. Details concerning the simulated model and the numerical simulations are presented in the Supplemental Material (SM) [45]. We have checked that variations of the model corresponding to different ways of accounting for the initial stability and the force balance lead to the same results (see SM [45]).

We first show that the model displays the same behavior as that found in numerical simulations of particle systems [3,19,20], with in particular the signature of a brittle-to-ductile transition accompanied by substantial finite-size effects [37,38]. In consequence, it provides a suitable framework to address the issues discussed above. In Fig. 1, we present stress-versus-strain curves for a 3D system with $L = 200$ for two values of the disorder strength, $R = 0.3$ and $R = 0.8$. The former clearly shows brittle yielding characterized by a discontinuous stress drop

and the appearance of a shear band (top inset), while the latter displays ductile yielding characterized by a continuous monotonic stress growth and homogeneously distributed plastic events (bottom inset). Brittle and ductile yieldings are thus qualitatively distinct, and their occurrence depends on the disorder strength R . The present results are in line with previous numerical observations in two-dimensional EPMs [40,42,55].

Our second goal is to identify the putative critical point separating brittle and ductile yielding. In previous studies [19,20,28], the maximum stress drop, $\langle \Delta\sigma_{\max} \rangle = \langle \max_{\gamma} \{ \Delta\sigma(\gamma) \} \rangle$ where $\Delta\sigma(\gamma)$ is the stress drop due to irreversible events at the strain γ , was used as an order parameter to detect the transition. Here, $\langle \dots \rangle$ denotes an average over many independent realizations (or samples), and the maximum is computed for each sample and then averaged over samples. We have found that for EPMs a more efficient order parameter is obtained from the fraction of sites along a single line in 2D or plane in 3D that have yielded at least once up to the strain γ . We consider the maximum of this fraction over all horizontal and vertical lines (2D) or planes (3D) and we call this quantity $n(\gamma)$. By construction it is an increasing function of γ . It shows a discontinuous jump of order $O(1)$ when $\sigma(\gamma)$ shows a discontinuous drop of order $O(1)$ and it increases continuously when $\sigma(\gamma)$ shows a continuous ductile behavior (see below). Therefore, $n(\gamma)$ essentially contains the same information as $\sigma(\gamma)$ for distinguishing brittle and ductile yielding behavior. We then define a new order parameter, $\Delta n_{\max} = \max_{\gamma} \{ \Delta n(\gamma) \}$, where $\Delta n(\gamma)$ is the jump of $n(\gamma)$ that takes place in the AQS dynamics from γ to $\gamma + \Delta\gamma$ in a given sample. We have observed that Δn_{\max} better quantifies the abrupt emergence of a system-spanning shear band and, as a result, detects the critical point in EPMs more accurately than $\Delta\sigma_{\max}$ (see the detailed discussion in SM [45]).

As seen in Figs. 2(a) and 2(b), the average order parameter $\langle \Delta n_{\max} \rangle$ is small and essentially constant at high disorder strength R and it starts to rapidly grow below some finite value of R . Moreover, as L increases both in 2D and in 3D, the increase of $\langle \Delta n_{\max} \rangle$ with decreasing R becomes steeper while the flat part becomes smaller, suggesting the presence of a critical point. Figures 2(c) and 2(d) show the variance of Δn_{\max} , which corresponds to the associated “disconnected susceptibility,” $\chi_{\text{dis}} = N \text{Var}(\Delta n_{\max})$, defined in analogy with an AQS driven random-field Ising model [19,21]. (It provides crisper, but similar, results than the “connected susceptibility” $\chi_{\text{con}} = -\partial \langle \Delta n_{\max} \rangle / \partial \gamma$ [19,20].) The disconnected susceptibility is strongly peaked and the peak becomes sharper and higher with increasing L , suggesting a divergence at some critical point. Essentially the same trend is observed for $\Delta\sigma_{\max}$ (see SM [45]), in agreement with the results of molecular simulations [19].

To firmly establish the existence of the critical point, we have performed a detailed finite-size scaling analysis.

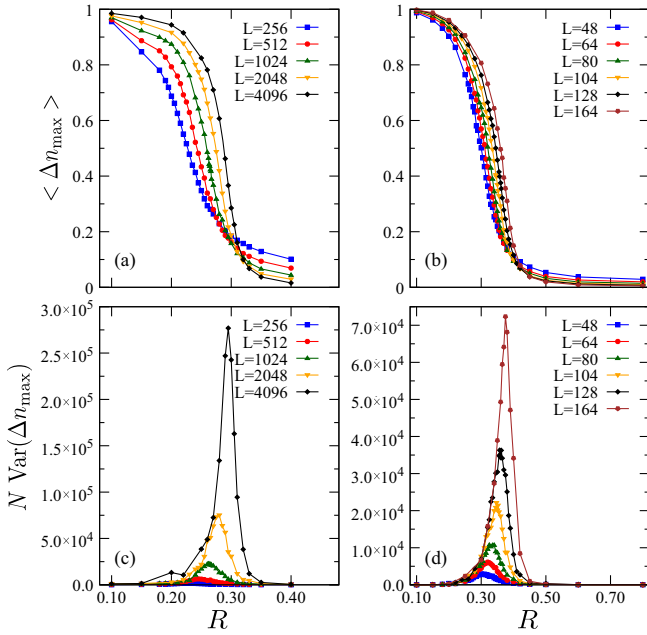


FIG. 2. Evidence for a critical point in 2D and 3D EPMs. Upper: average value of the order parameter $\langle \Delta n_{\max} \rangle$ as a function of R for several system sizes in 2D (a) and 3D (b). Lower: variance of Δn_{\max} multiplied by $N = L^D$, where D is the spatial dimensions, i.e., disconnected susceptibility, in 2D (c) and 3D (d).

We use here the same scaling ansatz as that of the AQS driven random-field Ising model, $\chi_{\text{dis}}(r, L) \sim L^{\bar{\gamma}/\nu} \Psi(rL^{1/\nu})$, where $R_c(L)$ locates the maximum value of χ_{dis} , $r = [R - R_c(L)]/R$ is the reduced disorder strength, $\Psi(\cdot)$ is a scaling function, and with $\bar{\gamma}$ and ν some critical exponents. According to this ansatz, the maximum over r of $\chi_{\text{dis}}(r, L)$ should diverge as $L^{\bar{\gamma}/\nu}$ and its full width at half maximum should vanish as $L^{-1/\nu}$. The corresponding plots obtained from the data in Figs. 2(c) and 2(d) are shown in Fig. 3. We observe a good power-law behavior, and by fitting these curves we obtain $\bar{\gamma}/\nu = 1.86 \pm 0.02$ and $\nu = 3.0 \pm 0.3$ in 2D, and $\bar{\gamma}/\nu = 2.66 \pm 0.04$ and $\nu = 2.5 \pm 0.2$ in 3D,

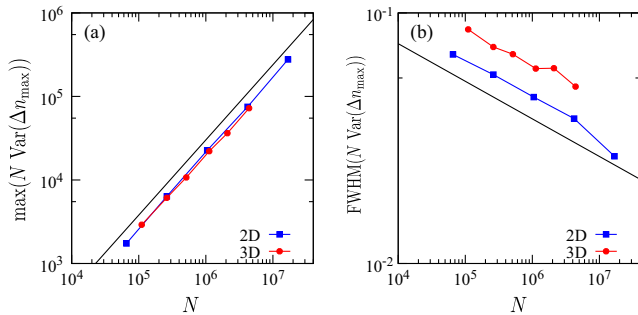


FIG. 3. Log-log plot of the maximum (a) and the full width at half maximum (b) of the disconnected susceptibility associated with the order parameter Δn_{\max} as a function of $N = L^D$ for both 2D (blue) and 3D (red). The straight black lines have slopes 0.9 in (a) and -0.15 in (b).

where the errors are derived from the fit. We also show in Fig. 4 the scaling collapse of the disconnected susceptibility, in which the parameters $\bar{\gamma}$, ν , and $R_c(L)$ are adjusted to provide the best visual collapse of the curves for the different values of L . The displayed collapses are for $\bar{\gamma}/\nu \approx 1.82$ and $\nu \approx 2.9$ in 2D, and $\bar{\gamma}/\nu \approx 2.61$ and $\nu \approx 2.2$ in 3D, values that are consistent with those determined by the fitting procedure. Work is now in progress to determine whether these critical exponents are in the same universality class as an AQS driven random-field Ising model with Eshelby-like interactions [56].

Figures 2–4 provide very strong evidence for a critical behavior around $R_c(L)$ with an estimate for the associated exponents $\bar{\gamma}$ and ν in 2D and 3D. However, the critical disorder $R_c(L)$ slightly shifts to larger R as L increases, as seen from Fig. 2. Understanding the fate of the critical disorder $R_c(L)$ in the thermodynamic limit is therefore a key issue. References [19,20] proposed that $R_c(L \rightarrow \infty)$ stays finite in the thermodynamic limit, whereas Refs. [36–38] argued that $R_c(L \rightarrow \infty) \rightarrow \infty$. Note that in this second scenario there is no ductile phase for large enough system size, i.e., all systems are brittle in the thermodynamic limit (except in the singular infinite-disorder limit). We stress that the existence of a finite-disorder brittle-to-ductile critical point in the thermodynamic limit is a separate issue from the persistence of an overshoot in the average stress-versus-strain curve for large ductile systems, which was the main concern of Ref. [37]. We show below that by disentangling these two problems one can obtain conclusive evidence in favor of the existence of the critical point in the thermodynamic limit.

We display in Fig. 5(a) the stress-versus-strain curves of typical 3D samples at fixed R for several values of L . We set $R = 0.40$ ($> R_c(L)$), which belongs to the putative ductile yielding regime as determined from the above finite-size scaling analysis. The plots focus on the stress values around the overshoot. For a fixed R , the stress drop tends to become sharper with increasing L , showing the same trend as found in Refs. [36–38]. Instead, as shown in

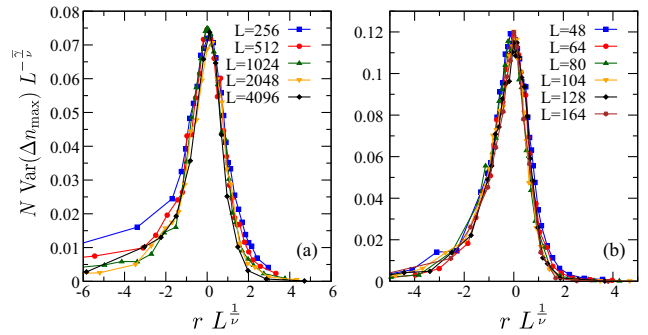


FIG. 4. Scaling plot of the disconnected susceptibility versus reduced disorder $r = [R - R_c(L)]/R$ for the data in Fig. 2 in 2D (a) and 3D (b) EPMs. A good collapse is obtained for $\bar{\gamma}/\nu \approx 1.82$ and $\nu \approx 2.9$ in 2D and $\bar{\gamma}/\nu \approx 2.61$ and $\nu \approx 2.2$ in 3D.

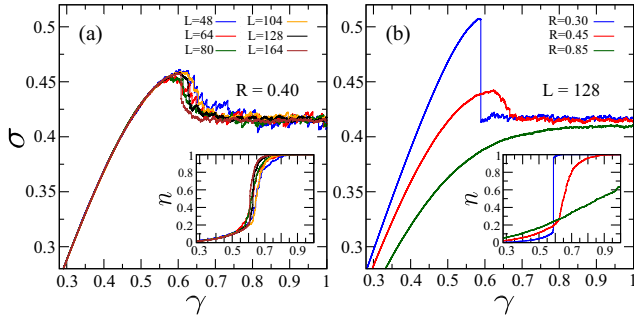


FIG. 5. Stress-versus-strain curves for 3D samples at fixed disorder strength $R = 0.40$ for several system sizes (a) and at fixed system size $L = 128$ for different values of R (b). Insets: The corresponding $n(\gamma)$ curves.

Fig. 5(b), for a fixed L (here, $L = 128$) a clear evolution between distinct yielding patterns is observed as R is decreased, from a purely monotonic increase of the stress to a continuous overshoot and then to a discontinuous drop. To characterize the asymptotic behavior when $L \rightarrow \infty$, we locate for each given system size L the value of R at which the overshoot first appears (coming from large R) in the average stress-versus-strain curves and we denote it by $R_o(L)$ (see SM [45] for details). We display R_o , together with the critical disorder R_c , for 2D and 3D in Fig. 6. To facilitate the comparison between 2D and 3D we plot R_o and R_c as a function of the number of sites $N = L^D$. We find that R_o is essentially independent of N in both cases while R_c increases very slowly with N . As we explain in more detail below, this is direct evidence for the existence of a ductile phase over a finite range of disorder strength in the thermodynamic limit.

The values of $R_o(N)$ and $R_c(N)$ define three distinct yielding regimes in the (N, R) plane, as schematically illustrated by the insets in Fig. 6. The region $R > R_o(N)$

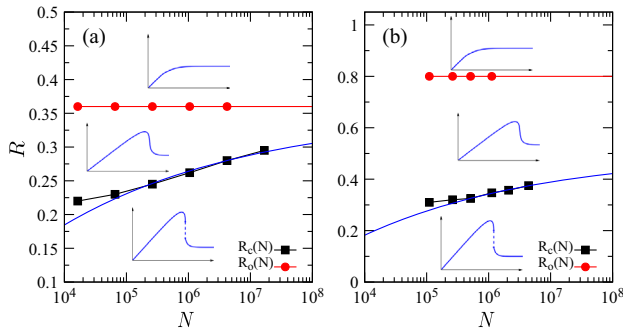


FIG. 6. Value of the disorder at which the overshoot first appears, R_o , and at the apparent critical point, R_c , as a function of the system size, $N = L^D$, in 2D (a) and in 3D (b). Blue lines are fits to $R_c^\infty - a/N^b$, with $R_c^\infty = 0.35$, $a = 0.61$, $b = 0.14$ in 2D and $R_c^\infty = 0.5$, $a = 1.29$, $b = 0.15$ in 3D. The parameter b is related to the critical exponent ν through $1/\nu = Db$, so that the fits yield $\nu \approx 3.57$ in 2D and $\nu \approx 2.22$ in 3D. Insets: The corresponding schematic stress-versus-strain curves.

corresponds to a monotonic increase of the average stress, with no overshoot. The region $R < R_c(N)$ corresponds to a discontinuous stress drop at yielding. The regime $R_c(N) < R < R_o(N)$ corresponds to a continuous average stress curve with a mild overshoot. By construction, $R_c(N)$ has to remain below $R_o(N)$, which then gives an upper bound on the critical disorder. The fact that $R_o(N)$ is essentially independent of N thus provides strong evidence that $R_c(N)$ converges to a finite value for large N and that a finite-disorder brittle-to-ductile critical point persists in the thermodynamic limit. The fate of the overshoot as $N \rightarrow \infty$ is instead unclear and depends on whether $R_c(N)$ converges to $R_o(\infty)$ or to $R_c(\infty) < R_o(\infty)$ in the thermodynamic limit. In the former case the overshoot disappears at the critical point whereas a regime of ductile yielding with an overshoot exists in the latter case. We show in Fig. 6 the best fits to $R_c(N) = R_c(\infty) - a/N^b$ with $R_c(\infty)$, a , and b free parameters. We find that $R_c(\infty)$ is finite in 2D and 3D. In the critical scaling picture and assuming that 2D and 3D are below the upper critical dimension, the parameter b is related to the (correlation length) exponent ν through $1/\nu = Db$. The fits then yield $\nu \approx 3.57$ in 2D and $\nu \approx 2.22$ in 3D, values which, given the large uncertainties, are consistent with the previous determinations given above.

Strictly speaking, we cannot exclude an alternative scenario in which $R_o(N)$ would start to increase with N above some size N^* which is out of reach of present-day simulations and would ultimately diverge in the thermodynamic limit together with $R_c(N)$. However, in view of the absence of any observable N dependence of $R_o(N)$ in the accessible range, which spans three decades in 2D, and of the lack of any sound theoretical argument supporting the existence of a critical size N^* , this possibility seems extremely unlikely.

In conclusion, we have performed extensive numerical simulations of athermally driven elastoplastic models in two and three dimensions. Thanks to the simple coarse-grained, lattice-based, nature of the modeling, we have been able to simulate substantially larger system sizes and larger number of samples than in molecular simulations, allowing us to perform a thorough finite-size scaling analysis. We have obtained clear evidence for the existence of a critical point separating brittle from ductile yielding in 2D and 3D and we have provided estimates for two associated critical exponents. Our results establish, at least for the studied elastoplastic models, that criticality persists in the thermodynamic limit and takes place for a finite value of the disorder characterizing the samples (and corresponding to a given initial stability of the solid), as suggested in Refs. [19,20]. The alternative scenario [36,38] according to which the critical point either takes place at infinite disorder or disappears because the disorder cannot go beyond some upper bound is not plausible in view of our results from elastoplastic modeling. It is nonetheless still unclear if the

overshoot in the average stress-versus-strain curve disappears in the thermodynamic limit for the ductile regime, as advocated in Ref. [37]. If it does, the critical point would occur exactly when the overshoot associated with brittle yielding disappears and then gives way to a monotonic (albeit singular at criticality) average stress-strain curve. The other possibility is that the critical point takes place at a value of the disorder for which a smooth overshoot is still present. The latter case implies that disorder, which is not accounted for in the linear instability argument of Ref. [37], is able to pin the propagation of the instability, thereby allowing for the presence of a smooth overshoot. It is hard to go beyond the present study in terms of numerical simulations. Thus, progress is now needed on the theoretical front.

Finally, we point out that the presence of a finite-disorder critical point is not restricted to the specific rheological setting considered in this Letter. Recently, the AQS cyclic shear protocol has been actively studied, in relation to other nonequilibrium phase transition phenomena such as absorbing-state phase transitions. This protocol also leads to a transition from ductile to brittle-like behavior, as a function of the disorder or stability of the initial glass samples, as shown in molecular simulations [27,28], simulated EPMs [55,57], as well as a mean-field EPM [58]. A detailed characterization of the critical point under cyclic shear and the determination of the associated exponents would be an interesting subject for future research.

We thank Ludovic Berthier, Chen Liu, Sylvain Patinet, and Matthieu Wyart for discussions. We also thank Chen Liu for multiple advices for the numerical implementation of the elastoplastic models. This work was granted access to the HPC resources of the MeSU platform at Sorbonne Université and the HPC resources of MesoPSL financed by the Region Ile de France and the project Equip@Meso (reference ANR-10-EQPX-29-01) of the programme Investissements d’Avenir supervised by the Agence Nationale pour la Recherche. This project has received funding from the European Research Council (ERC) under the European Union’s Horizon 2020 research and innovation program (Grant Agreement No. 723955–GlassUniversality) and from the Simons Foundation (Grant No. 454935 to G. B.; Grant No. 454955 to F. Z.).

*Corresponding author.

saverio.rossi@sorbonne-universite.fr

- [1] A. Nicolas, E. E. Ferrero, K. Martens, and J.-L. Barrat, *Rev. Mod. Phys.* **90**, 045006 (2018).
 [2] J.-L. Barrat and A. Lemaitre, in *Dynamical Heterogeneities in Glasses, Colloids, and Granular Media*, edited by L. Berthier, G. Biroli, J.-P. Bouchaud, L. Cipelletti, and W. van Saarloos (Oxford University Press, New York, 2011).

- [3] D. Rodney, A. Tanguy, and D. Vandembroucq, *Model. Simul. Mater. Sci. Eng.* **19**, 083001 (2011).
 [4] D. Bonn, M. M. Denn, L. Berthier, T. Divoux, and S. Manneville, *Rev. Mod. Phys.* **89**, 035005 (2017).
 [5] M. L. Falk and J. S. Langer, *Annu. Rev. Condens. Matter Phys.* **2**, 353 (2011).
 [6] G. Kumar, P. Neibecker, Y. H. Liu, and J. Schroers, *Nat. Commun.* **4**, 1536 (2013).
 [7] M. Vasoya, C. H. Rycroft, and E. Bouchbinder, *Phys. Rev. Appl.* **6**, 024008 (2016).
 [8] M. Fan, M. Wang, K. Zhang, Y. Liu, J. Schroers, M. D. Shattuck, and C. S. O’Hern, *Phys. Rev. E* **95**, 022611 (2017).
 [9] S. Karmakar, E. Lerner, and I. Procaccia, *Phys. Rev. E* **82**, 055103(R) (2010).
 [10] A. Lemaitre, C. Mondal, M. Moshe, I. Procaccia, S. Roy, and K. Sreiber-Re’em, *Phys. Rev. E* **104**, 024904 (2021).
 [11] J. Lin, T. Gueudré, A. Rosso, and M. Wyart, *Phys. Rev. Lett.* **115**, 168001 (2015).
 [12] A. Wisitsorasak and P. G. Wolynes, *Proc. Natl. Acad. Sci. U.S.A.* **109**, 16068 (2012).
 [13] C. Rainone, P. Urbani, H. Yoshino, and F. Zamponi, *Phys. Rev. Lett.* **114**, 015701 (2015).
 [14] P. Urbani and F. Zamponi, *Phys. Rev. Lett.* **118**, 038001 (2017).
 [15] P. K. Jaiswal, I. Procaccia, C. Rainone, and M. Singh, *Phys. Rev. Lett.* **116**, 085501 (2016).
 [16] G. Parisi, I. Procaccia, C. Rainone, and M. Singh, *Proc. Natl. Acad. Sci. U.S.A.* **114**, 5577 (2017).
 [17] E. De Giuli, *Phys. Rev. E* **101**, 043002 (2020).
 [18] C. E. Maloney and A. Lemaitre, *Phys. Rev. E* **74**, 016118 (2006).
 [19] M. Ozawa, L. Berthier, G. Biroli, A. Rosso, and G. Tarjus, *Proc. Natl. Acad. Sci. U.S.A.* **115**, 6656 (2018).
 [20] M. Ozawa, L. Berthier, G. Biroli, and G. Tarjus, *Phys. Rev. Res.* **2**, 023203 (2020).
 [21] S. Rossi and G. Tarjus, *J. Stat. Mech.* (2022) 093301.
 [22] J. P. Sethna, K. A. Dahmen, and C. R. Myers, *Nature (London)* **410**, 242 (2001).
 [23] S. K. Nandi, G. Biroli, and G. Tarjus, *Phys. Rev. Lett.* **116**, 145701 (2016).
 [24] O. Dauchot, S. Karmakar, I. Procaccia, and J. Zylberg, *Phys. Rev. E* **84**, 046105 (2011).
 [25] J. Ketkaew, W. Chen, H. Wang, A. Datye, M. Fan, G. Pereira, U. D. Schwarz, Z. Liu, R. Yamada, W. Dmowski *et al.*, *Nat. Commun.* **9**, 3271 (2018).
 [26] Y. Jin, P. Urbani, F. Zamponi, and H. Yoshino, *Sci. Adv.* **4**, eaat6387 (2018).
 [27] W.-T. Yeh, M. Ozawa, K. Miyazaki, T. Kawasaki, and L. Berthier, *Phys. Rev. Lett.* **124**, 225502 (2020).
 [28] H. Bhaumik, G. Foffi, and S. Sastry, *Proc. Natl. Acad. Sci. U.S.A.* **118**, e2100227118 (2021).
 [29] A. Barbot, M. Lerbinger, A. Lemaitre, D. Vandembroucq, and S. Patinet, *Phys. Rev. E* **101**, 033001 (2020).
 [30] H. Borja da Rocha and L. Truskinovsky, *Phys. Rev. Lett.* **124**, 015501 (2020).
 [31] S. Sastry, *Phys. Rev. Lett.* **126**, 255501 (2021).
 [32] R. Benzi, T. Divoux, C. Barentin, S. Manneville, M. Sbragaglia, and F. Toschi, *Phys. Rev. E* **104**, 034612 (2021).
 [33] J. S. Langer, *Phys. Rev. E* **101**, 063004 (2020).

- [34] D. Richard, E. Lerner, and E. Bouchbinder, *MRS Bull.* **46**, 902 (2021).
- [35] F. Arceri, E. I. Corwin, and V. F. Hagh, *Phys. Rev. E* **104**, 044907 (2021).
- [36] H. J. Barlow, J. O. Cochran, and S. M. Fielding, *Phys. Rev. Lett.* **125**, 168003 (2020).
- [37] J. Pollard and S. M. Fielding, *Phys. Rev. Research* **4**, 043037 (2022).
- [38] D. Richard, C. Rainone, and E. Lerner, *J. Chem. Phys.* **155**, 056101 (2021).
- [39] G. Picard, A. Ajdari, F. Lequeux, and L. Bocquet, *Eur. Phys. J. E* **15**, 371 (2004).
- [40] M. Popović, T. W. J. de Geus, and M. Wyart, *Phys. Rev. E* **98**, 040901(R) (2018).
- [41] J.-C. Baret, D. Vandembroucq, and S. Roux, *Phys. Rev. Lett.* **89**, 195506 (2002).
- [42] D. Vandembroucq and S. Roux, *Phys. Rev. B* **84**, 134210 (2011).
- [43] J. Lin, E. Lerner, A. Rosso, and M. Wyart, *Proc. Natl. Acad. Sci. U.S.A.* **111**, 14382 (2014).
- [44] J. D. Eshelby, *Proc. R. Soc. A* **241**, 376 (1957).
- [45] See Supplemental Material at <http://link.aps.org/supplemental/10.1103/PhysRevLett.129.228002> for the implementation of the elastoplastic models, the comparison with molecular dynamics, the definition of the order parameter, the discussion about force balance, some variations of the model, and the determination of the onset of the stress overshoot, which includes Refs. [46–54].
- [46] E. Agoritsas, E. Bertin, K. Martens, and J.-L. Barrat, *Eur. Phys. J. E* **38**, 71 (2015).
- [47] A. Barbot, M. Lerbinger, A. Hernandez-Garcia, R. García-García, M. L. Falk, D. Vandembroucq, and S. Patinet, *Phys. Rev. E* **97**, 033001 (2018).
- [48] E. E. Ferrero and E. A. Jagla, *Soft Matter* **15**, 9041 (2019).
- [49] T. Mura, *Micromechanics of Defects in Solids* (Springer Science & Business Media, New York, 2013).
- [50] C. Liu, S. Dutta, P. Chaudhuri, and K. Martens, *Phys. Rev. Lett.* **126**, 138005 (2021).
- [51] D. F. Castellanos, S. Roux, and S. Patinet, *C. R. Phys.* **22**, 135 (2021).
- [52] G. Zhang, H. Xiao, E. Yang, R. J. Ivancic, S. A. Ridout, R. A. Riggelman, D. J. Durian, and A. J. Liu, [arXiv:2205.08678](https://arxiv.org/abs/2205.08678).
- [53] J.-Y. Fortin and M. Clusel, *J. Phys. A* **48**, 183001 (2015).
- [54] C. Liu, Critical dynamics at the yielding transition and creep behavior of amorphous systems: Mesoscopic modeling, Ph.D. thesis, Université Grenoble Alpes, 2016.
- [55] C. Liu, E. E. Ferrero, E. A. Jagla, K. Martens, A. Rosso, and L. Talon, *J. Chem. Phys.* **156**, 104902 (2022).
- [56] S. Rossi, M. Ozawa, G. Biroli, and G. Tarjus (to be published).
- [57] D. Kumar, S. Patinet, C. E. Maloney, I. Regev, D. Vandembroucq, and M. Mungan, *J. Chem. Phys.* **157**, 174504 (2022).
- [58] J. T. Parley, S. Sastry, and P. Sollich, *Phys. Rev. Lett.* **128**, 198001 (2022).